AGU PUBLICATIONS

JGR

Journal of Geophysical Research: Space Physics

RESEARCH ARTICLE
10.1002/2014JA020465

Key Points:
- Multipoint Cluster observations of a solar wind reconnection exhaust
- ACE and Wind observations show that the current sheet is large scale and planar
- Exhaust has small-scale folds orthogonal to the reconnection plane

Correspondence to:
R. Mistry,
rishi.mistry09@imperial.ac.uk

Citation:
Mistry, R., J. P. Eastwood, and H. Hietala (2015), Detection of small-scale folds at a solar wind reconnection exhaust, *J. Geophys. Res. Space Physics*, *120*, 30–42, doi:10.1002/2014JA020465.

Received 1 AUG 2014
Accepted 9 DEC 2014
Accepted article online 12 DEC 2014
Published online 19 JAN 2015

Detection of small-scale folds at a solar wind reconnection exhaust

R. Mistry[1], J. P. Eastwood[1], and H. Hietala[1]

[1]Space and Atmospheric Physics, Blackett Laboratory, Imperial College London, London, UK

Abstract Observations of reconnection in the solar wind over the last few years appear to indicate that the majority of large-scale reconnecting current sheets are roughly planar, and that reconnection itself is quasi-steady. Most studies of solar wind exhausts have used spacecraft with large separations and relatively low time cadence ion measurements. Here we present multipoint Cluster observations of a reconnection exhaust and the associated current sheet at ACE and Wind, enabling it to be studied on multiple length scales and at high time resolution. While analysis shows that on large scales the current sheet is planar, detailed measurements using the four closely spaced Cluster spacecraft show that the trailing edge of the reconnection jet is nonplanar with folds orthogonal to the reconnection plane, with length scales of approximately 230 ion inertial lengths. Our findings thus suggest that while solar wind current sheets undergoing reconnection may be planar on large scales, they may also exhibit complex smaller-scale structure. Such structure is difficult to observe and has rarely been detected because exhausts are rapidly convected past the spacecraft in a single cut; there is therefore a limited set of spacecraft trajectories through the exhaust which would allow the nonplanar features to be intercepted. We consider how such nonplanar reconnection current sheets can form and the processes which may have generated the 3-D structure that was observed.

1. Introduction

Magnetic reconnection is a process that changes the magnetic topology of a plasma and converts stored magnetic energy into particle energies [e.g., *Vasyliunas*, 1975]. This process is of great importance to many astrophysical and laboratory plasmas. In many space plasma environments magnetic reconnection is commonly thought of as having a quasi 2-D geometry in which field lines from different magnetic domains reconnect in the diffusion region, forming Alfvénic exhausts which accelerate plasma away from the X line [*Zweibel and Yamada*, 2009]. The importance of the third dimension, however, has been emphasized more recently as it may add further complexity to the exhaust structure and reconnection dynamics [e.g., *Yin et al*., 2008; *Daughton et al*., 2011].

The solar wind provides an excellent environment to study the properties of reconnection exhausts because the boundary conditions are effectively "open," unlike at the magnetopause or magnetotail where reconnection process may be constrained by magnetospheric boundary conditions [*Gosling*, 2012]. Furthermore, they are rapidly convected past the spacecraft by the solar wind; this typically allows measurements to be taken across the exhaust over time scales during which the exhaust is not expected to evolve considerably. Solar wind reconnection exhausts were first conclusively identified in ACE spacecraft data. They were identified by a significant change in the magnetic field direction which was accompanied by a depression in the field magnitude and accelerated ion flow. Enhanced ion temperatures and densities were also evident as a result of interpenetrating ion beams across the exhausts [*Gosling et al*., 2005].

Multispacecraft observations of solar wind reconnection exhausts have indicated that exhausts often form roughly planar, quasi-steady, and large-scale structures. Observations of the same reconnection exhaust at ACE, Wind, and Cluster were used to demonstrate that the reconnecting current sheet was planar over these distances and the authors inferred that the X line extended at least 390 R_E (Earth radii) [*Phan et al*., 2006]. *Davis et al*. [2006] confirmed that bidirectional jets emanate from the diffusion region by directly observing two oppositely directed jets that were directed away from a common source region and showed that the exhausts had a planar geometry. Furthermore, based on a statistical study of 51 reconnection exhausts from ACE and Wind data, it was inferred that the reconnection X lines were extended, in some cases in excess of

100 R_E, and that the reconnection current sheets were typically planar over this extent, as expected from a 2-D reconnection geometry [*Phan et al*., 2009].

Large-scale reconnecting current sheets in the solar wind therefore appear to be planar even though the solar wind is inherently turbulent. Simulations of reconnection in stochastically turbulent media have typically shown that the turbulent magnetic field results in reconnection at multiple X lines and hence an enhanced reconnection rate [*Kowal et al*., 2009; *Lazarian and Vishniac*, 1999]. Although the implications of this on the geometry of the exhausts downstream of the X line have not been fully elucidated, this might imply that the 3-D geometry of solar wind reconnection exhausts are further complicated in reality.

Evidence for a complex 3-D geometry may have been present in Ulysses data, where variability in multiple magnetic field components across several exhausts was suggested to be caused by traversals of nonplanar exhaust boundaries [*Gosling et al*., 2006]. Direct observations of nonplanar exhausts, however, are rare. Multiple encounters of three out of five spacecraft with an exceptionally thick exhaust (where the five spacecraft took a total of 5 h to traverse the exhaust) at the heliospheric current sheet indicated that the boundaries of the exhaust were nonplanar over length scales of tens of Earth radii (thousands of ion inertial lengths) [*Gosling et al*., 2007b], while multiple spacecraft encounters with an exhaust where the X line was inferred to be in excess of 670 R_E indicated nonplanar length scales of a few Earth radii (hundreds of ion inertial lengths) [*Gosling et al*., 2007c].

The Solar Wind Electron Proton Alpha Monitor (SWEPAM) instrument on the ACE spacecraft [*McComas et al*., 1998] provides ion plasma moments with a 64 s time cadence; therefore, measurements of accelerated ion flow (a fundamental signature of reconnection) cannot be made across relatively thin current sheets using ACE data. Single spacecraft observations using the 3-D Plasma and Particle Investigation (3DP) 3 s cadence ion instrument on Wind [*Lin et al*., 1995] have identified far thinner exhausts (typically observed over intervals of tens of seconds) than those which were resolved by ACE. These exhausts have a much higher occurrence rate (approximately 1–3 exhausts per day at Wind [*Gosling*, 2012], although higher rates were recorded by *Osman et al*. [2014] (using a different method)) and frequently have a low magnetic shear [e.g., *Gosling et al*., 2007a; *Gosling and Phan*, 2013]. *Gosling* [2007] observed thin reconnection exhausts in the high-speed solar wind using Wind. Although such thin current sheets should be resolvable using the ACE magnetometer, the current sheets associated with the exhausts at Wind (which had a maximum separation from ACE of 125 R_E) could not be identified in ACE magnetometer data. This suggests that thin current sheets that reconnect in high-speed turbulent solar wind are not large scale and do not form extended reconnection X lines.

It is not known whether the thin, strong guide field exhausts observed by Wind can also form extended planar structures as is common for thick exhausts, and whether they have more complex geometries. Particle-in-cell (PIC) reconnection simulations [e.g., *Lapenta and Brackbill*, 2002; *Fujimoto*, 2009] have demonstrated that folds can form along current sheets as a result of plasma instabilities; however, such small-scale perturbations from a planar geometry have not yet been confirmed by in situ measurements. Here we present a reconnection event observed by Cluster where we use the four spacecraft to constrain the geometry of the reconnection exhaust. A complete exhaust traversal is followed by two reentries into the exhaust by each of the four spacecraft. Examination of the magnetic field, ion velocities, and timing analysis suggests that the incomplete traversals are a result of small-scale folds in the trailing edge of the jet. Observations of the same current sheet at ACE and Wind indicate that the current sheet is large scale and planar. Ion velocities cannot be resolved across the current sheet at ACE; however, data from Wind indicate that the reconnection exhaust may be present there.

2. Observations

2.1. Overview

On 17 January 2002 the four Cluster spacecraft [*Escoubet et al*., 2001] were arranged in an approximately straight line in the solar wind with interspacecraft separations of approximately 0.5 R_E, (see Figure 1). While this spacecraft formation is not conducive to traditional multispacecraft timing analysis which can be used to determine the orientation of a planar boundary [*Dunlop and Woodward*, 1998], it is still possible to use the four spacecraft data to apply constraints to a boundary which propagates past the spacecraft.

Magnetic field data were obtained by the Cluster Magnetic Field Investigation instrument at 22 vectors s^{-1} [*Balogh et al*., 2001], and ion plasma moments are taken at a time cadence of 4 s by the Cluster Ion

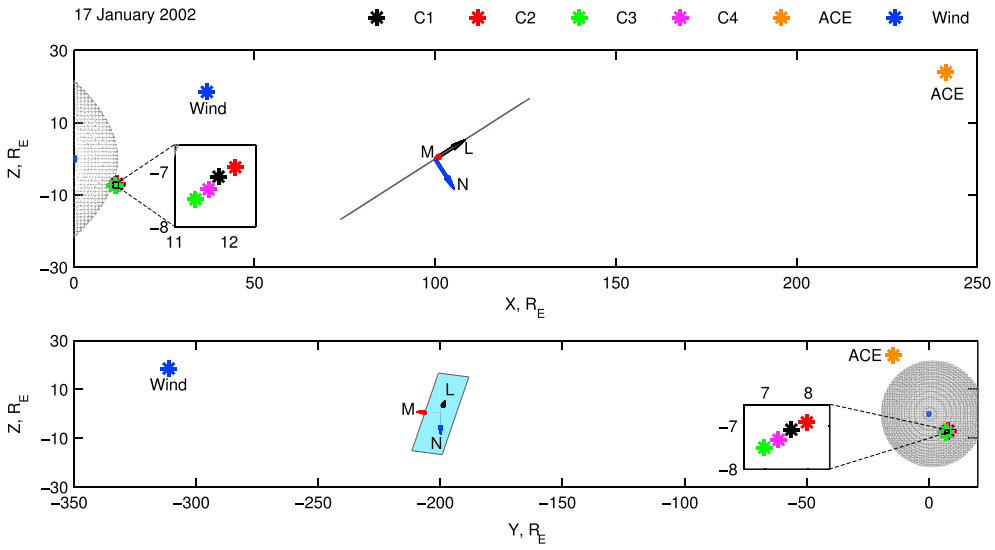

Figure 1. Positions of Cluster, ACE, and Wind when they observed the current sheet. The bow shock (calculated using the *Merka et al.* [2005] model and an upstream density of 12.5 cm^{-3}, velocity of 402 km s^{-1}, and magnetic field strength of 6.7 nT) is shown in grey. The *LMN* directions and the associated current sheet are shown, at an arbitrary position. The formation of the Cluster spacecraft is shown in more detail in both panels.

Spectrometry Hot Ion Analyser (CIS-HIA) [*Reme et al.*, 2001]. CIS-HIA does not discriminate between ion species, and measurements are only available from Cluster 1 and Cluster 3 (C1 and C3, respectively). At the time of observations the instrument was in a magnetospheric (i.e., not solar wind) mode; therefore, temperature and density moments should be handled with caution. We instead use electron densities derived from wave measurements of the plasma frequency from Whisper [*Décréau et al.*, 1999], and references from hereon to Cluster density measurements refer to these electron densities. Whisper data are available at a time cadence of 1.7 s.

Figure 2 shows the magnetic field, electron density, and ion velocity observed by C3 during a 12 min interval when the spacecraft was located within the solar wind. Between 09:40:10 UT and 09:40:55 UT (interval 1) the magnetic field direction changed considerably (evidenced by the change in sign of B_x and B_z), indicating the presence of a solar wind current sheet. During the current sheet crossing the field strength decreased, the density increased, and there was a deflection of the ion velocity. Changes in the magnetic field direction and changes which are somewhat similar to those seen during interval 1 in the field magnitude, density and ion velocity are also evident between 09:41:12 UT and 09:41:32 UT (interval 2) and between 09:42:19 UT and 09:42:49 UT (interval 3). We note that prior to 09:34:00 UT, Cluster was located in the ion foreshock where the ion velocity and magnetic field were variable. During the interval of interest, however, ion foreshock activity was not present. The spacecraft was located within the electron foreshock; however, this is not expected to affect the observations shown here nor affect the exhaust structure which we observe. Intervals 1–3 are uniquely identified for each Cluster spacecraft by identifying similar changes in the field magnitude, field direction, density, and ion velocity (where available) to the changes observed by C3.

Figure 3 shows the current sheet encounter in more detail, using a hybrid minimum variance coordinate system [*Gosling and Phan*, 2013]. *N* (the current sheet normal) is determined by $(\mathbf{B}_1 \times \mathbf{B}_2)/|\mathbf{B}_1 \times \mathbf{B}_2|$ where $\mathbf{B}_1$ and $\mathbf{B}_2$ are the initial and final magnetic field vectors of interval 1, respectively. The guide field direction, *M*, is determined by the cross product of *L′* and *N*, where *L′* is the maximum variance direction obtained from minimum variance analysis of the interval [*Sonnerup and Cahill*, 1967]. The exhaust outflow direction, *L*, is the cross product of *M* and *N*. Hybrid minimum variance coordinates were also determined from each Cluster spacecraft's traversal of the current sheet. The largest angular difference between any of the derived vectors was 8.6° in the *L* direction between C2 and C3. The coordinate systems derived from each spacecraft are therefore largely consistent, and we show all spacecraft observations in the coordinate system derived from C3 (see Table 1).

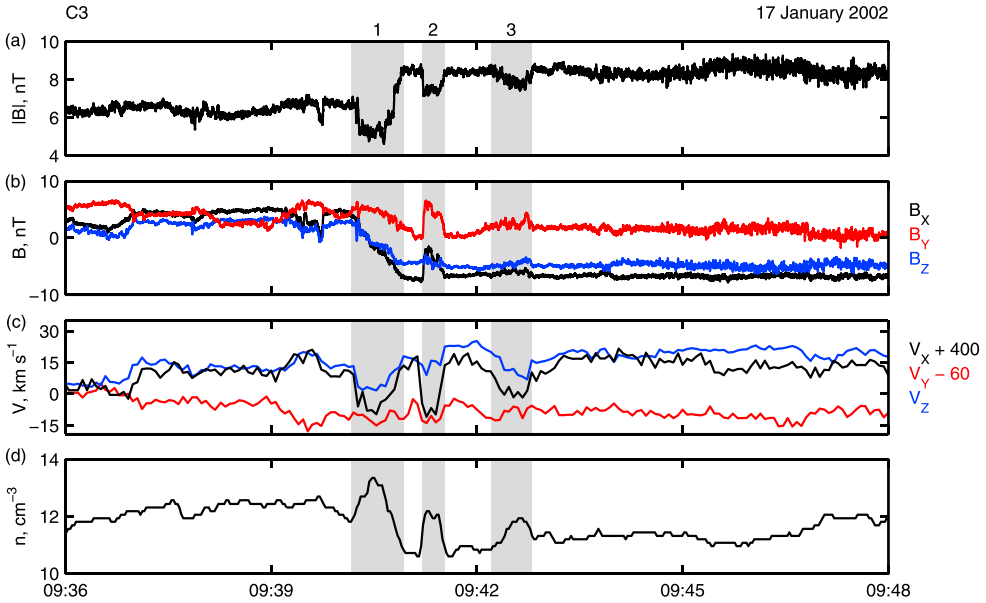

Figure 2. C3 observations of (a) magnetic field magnitude, (b) GSE components of the magnetic field, (c) GSE components of the ion velocity, (d) electron density derived from Whisper plasma wave measurements. Intervals 1–3 are shaded in grey.

Figure 3 shows a clear decrease in the field magnitude across interval 1 in observations at both C1 and C3. This is accompanied by a rotation in the field in the L component, while B_N is small and B_M is approximately constant, resulting in a magnetic shear angle of 122° across the interval at both spacecraft. The current sheet is not bifurcated, as is often observed in solar wind reconnection exhausts; the current sheet exhibits a relatively smooth rotation in the magnetic field. The density is increased in the current sheet. The magnetic field and density were not symmetric on either side of the exhaust; observations before the exhaust at C3 show $B = 6.6$ nT and $n = 11.9$ cm^{-3}, while $B = 8.5$ nT and $n = 10.7$ cm^{-3} afterward. There is accelerated ion flow in the $-L$ direction at both spacecraft. These observations are consistent with the presence of a reconnection

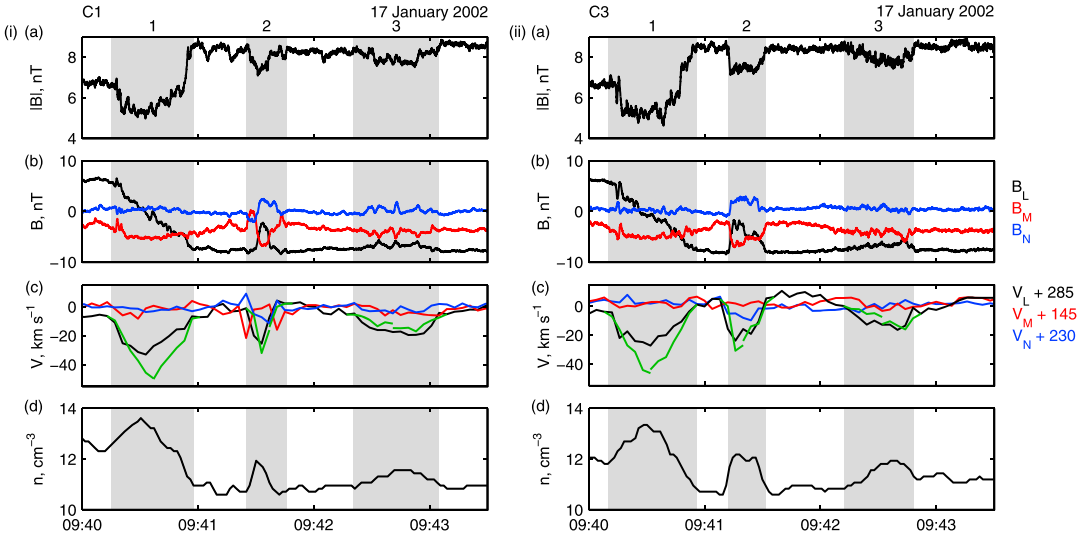

Figure 3. C1 (i) and C3 (ii) observations of (a) magnetic field magnitude, (b) magnetic field in *LMN* local current sheet normal coordinates, and (c) *LMN* ion velocity components. The *L* component of the Walen predicted exhaust velocity is shown in green for intervals 1–3. (d) Electron density derived from Whisper plasma wave measurements. Intervals 1–3 are shaded in grey for each spacecraft.

Table 1. *LMN* Coordinates Derived From Hybrid Minimum Variance Analysis of Magnetic Field Data From C3[a]

	X	*Y*	*Z*
L	0.79	0.25	0.56
M	0.24	−0.97	0.08
N	0.56	0.07	−0.82

[a]Expressed in GSE coordinates.

exhaust during interval 1 with the X line located in the +*L* direction relative to the spacecraft. Furthermore, we show the exhaust velocity predicted by the Walen relation [*Hudson*, 1970; *Paschmann et al.*, 1986] at both spacecraft. This velocity is calculated from reference points at either end of the interval (the two velocity profiles calculated from either end do not necessarily meet in the center of the current sheet) and is given by

$$\boldsymbol{v} = \boldsymbol{v}_1 \pm \left(\sqrt{\frac{1-\alpha}{\mu_0 \rho}}\boldsymbol{B} - \sqrt{\frac{1-\alpha_1}{\mu_0 \rho_1}}\boldsymbol{B}_1 \right)$$

where α is half the difference between the parallel and perpendicular plasma betas, ρ is the plasma density, and μ_0 is the permeability of free space. Values at the reference point are indicated by the subscript 1. CIS-HIA was in a magnetospheric mode, and temperature anisotropy measurements are unreliable. The expected velocities (in which we assume that the plasma is isotropic, i.e., $\alpha = 0$) and observed velocities agree reasonably well close to the leading and trailing edges of the exhaust; however, the observed velocity only reached 61% and 57% of the maximum predicted velocity at C1 and C3, respectively. The exhaust was swept over C3 by the solar wind over an interval of 46 s, indicating an exhaust width of 1.49 R_E (135 d_i, where d_i is the ion inertial length for $n = 11\ \mathrm{cm}^{-3}$), calculated using $(V_{SW} \cdot N)\delta t$ (where V_{SW} is the solar wind velocity, N is the normal to the current sheet, and $\delta t = 46$ s).

2.2. Large-Scale Structure

We now examine the context of these observations. Figure 4 shows an interval during which ACE and Wind observe similar changes in the magnetic field direction to the change observed by Cluster during interval 1. Comparison of magnetic field and plasma data between ACE, Wind, and Cluster over several hours shows that the spacecraft observe similar structures in the solar wind, and that these are observations of the same current sheet. ACE was located almost directly upstream of Cluster, while Wind was separated by ~300 R_E from Cluster along the $-Y_{GSE}$ direction (locations are shown in Figure 1). Hybrid minimum variance analysis was also applied to magnetic field data from ACE and Wind to identify the local current sheet normal at their

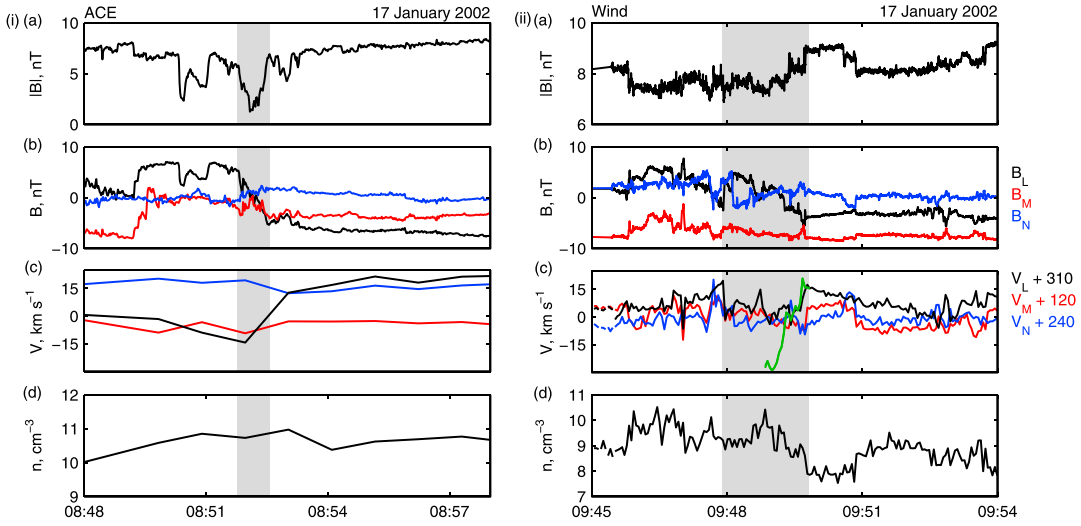

Figure 4. ACE (i) and Wind (ii) observations of (a) magnetic field magnitude, (b) *LMN* magnetic field components, and (c) *LMN* ion velocity components. The *L* component of the Walen predicted exhaust velocity for the second half of the current sheet is shown in green for Wind. (d) Ion density. The shaded interval indicates the current sheet that is associated with interval 1.

locations. The differences between the normal obtained from C3 and those obtained from ACE and Wind were 17° and 24°, respectively. This local analysis demonstrates that the current sheet is approximately planar on the length scales that separate Cluster, ACE, and Wind. The difference between the current sheet normal obtained from multispacecraft discontinuity timing analysis [*Horbury et al.*, 2001] between C3, ACE, and Wind and the normal at C3 is 4°. Furthermore, the difference between the predicted time lag between observations at ACE and C3 (based on the solar wind velocity and current sheet normal from C3) and the observed time lag is 129 s (4.4% of the observed time lag), while between ACE and Wind the difference is 274 s (7.8% of the observed time lag), which provides additional evidence that the current sheet is planar on large scales and that the spacecraft did indeed all observe the same current sheet.

As noted above, the ACE SWEPAM instrument has a 64 s resolution and is therefore unable to resolve the ion velocity across the current sheet. The 3DP 3 s resolution instrument on board Wind can resolve the ion density and ion velocity across the current sheet (Figure 4). There is a slight enhancement in the ion density and an increase in the velocity in the $-L$ direction. Across the current sheet the decrease in the field magnitude is weak and there is a strong guide field of ~7 nT; the magnetic shear angle is 54°. The magnetic field is relatively stable after the current sheet; however, it is significantly more variable prior to the arrival of the current sheet. A suitably defined reference point for the Walen relation could not be selected, and we only show the predicted velocity calculated from the reference point at the trailing edge, assuming that the plasma is isotropic (measurements from Wind Solar Wind Experiment [*Ogilvie et al.*, 1995] indicate that the surrounding plasma is approximately isotropic). There is strong agreement between the predicted and observed velocities until $B_L = 0$, and the observed velocity reached 44% of the maximum predicted velocity in the center of the current sheet. These observations suggest that Wind detected the same current sheet as that at Cluster and that the reconnection exhaust may have been present at Wind; however, at Wind the magnetic field was significantly more variable and the current sheet had a stronger guide field. *Gosling et al.* [2007c] similarly observed a varying guide field (magnetic shear angles of between 95° and 146°) at each of five spacecraft which observed the same reconnection exhaust, where the spacecraft spanned 668 R_E in the X line direction. During the event discussed in this paper, Cluster and ACE were located at a similar position along the X line (M) direction and Cluster was separated from Wind by a distance of 320 R_E (29,000 d_i) along the X line. Furthermore, the current sheet is thicker at Wind; ACE, C3, and Wind each encountered the exhaust for a period of 48 s, 46 s, and 115 s. Exhausts are expected to broaden with increasing distance from the diffusion region. ACE is 42 R_E closer to the diffusion region than Cluster (i.e., separated by 42 R_E in the $+L$ direction), while Wind was 11 R_E further away; therefore, the increased current sheet width at Wind is likely to be a consequence of the current sheet width varying along the X line rather than a result of exhaust broadening. Observations similar to intervals 2 and 3 could not be identified at ACE or Wind.

2.3. Reconnection Exhaust Structure at Cluster

We now examine the Cluster observations in more detail. The Cluster observations are of special interest as the reconnection exhaust was detected by the spacecraft 2 further times (intervals 2 and 3), despite being rapidly convected past the spacecraft by the solar wind. During interval 2, Figure 3 shows that there is a decrease in the field magnitude and increase in the density at both spacecraft. The ion speed is also increased, primarily in the $-L$ direction (although there is variability in V_M at C1). The maximum observed velocity within the interval is 80% and 81% of the predicted velocity (assuming isotropy) at C1 and C3, respectively. At the beginning of interval 2, C3 observed a change in B_L from −8.4 nT to −2.4 nT, followed by a gradual return to −8.4 nT. At both spacecraft the density, magnetic field strength, and magnetic field direction are very similar before and after interval 2, showing that Cluster did not return to the plasma environment which was present before the current sheet encounter. Indeed, since B_L remained negative, this indicates that the spacecraft reentered the exhaust, but that they did not cross the point in the exhaust at which $B_L = 0$. The similarity between ion velocity measurements at C3 during intervals 1 and 2 indicates that the intervals are due to reentries into the same exhaust. The spacecraft therefore traversed the trailing edge of the exhaust to reenter the exhaust at the beginning of interval 2, and traversed it again to exit the exhaust at the end of the interval. During this interval there were also changes in B_M and B_N, indicating that the orientation of the current sheet was slightly different between intervals 1 and 2. We are not able to accurately determine this orientation at interval 2 through minimum variance analysis as the current sheet is not completely traversed during the interval and the eigenvalues were not well separated. The variability

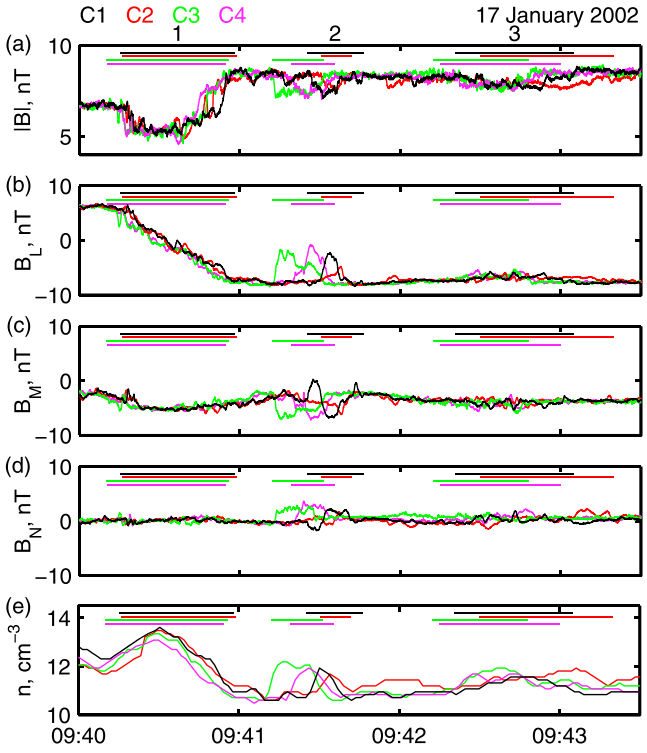

Figure 5. (a) Magnetic field magnitude. (b–d) *LMN* magnetic field components. (e) Electron density derived from Whisper plasma wave measurements. Horizontal lines in each panel indicate intervals 1–3 for each spacecraft.

in the *M* and *N* components of the magnetic field and velocity at C1 may indicate the presence of additional local small-scale structure within the exhaust.

During interval 3, there are weak changes in the magnetic field components. There is a decrease in the field magnitude of ~1 nT at C1 and C3 and an increase in the density of 0.6 cm^{-3} at C1 and 0.9 cm^{-3} at C3. There is an increased velocity in the $-L$ direction which is within strong agreement to that predicted for an exhaust by the Walen relation (assuming isotropy). Observed velocities at both spacecraft during interval 3 and the edges of interval 2 are similar to, but slightly less than, the Walen velocities. PIC simulations [*Le et al.*, 2014; *Liu et al.*, 2012] have similarly noted that the Walen prediction underestimates velocities at exhaust boundaries and overestimates velocities toward more central regions of the exhaust (as observed here at the centers of intervals 1 and 2). Although changes in individual field components are small, the increased density, decreased field magnitude, and observed velocity changes (and their agreement with the predicted changes) clearly indicate that the spacecraft have again reentered the exhaust. During this interval, however, they do not appear to have penetrated very deeply into the exhaust as the change in B_L (+2.3 nT at C3) is far smaller than in interval 2. Additionally, the density, field magnitude, and field direction on either side of the interval are similar to that observed after interval 1 and either side of interval 2, suggesting that interval 3 was again a result of traversals of the trailing edge of the exhaust.

High-resolution magnetic field data and densities from all four spacecraft are shown in Figure 5. The times at which each spacecraft is identified as being located within the exhaust are shown with horizontal bars. The magnetic field signatures are similar during interval 1, whereas during interval 2 C2 observes a smaller change in the magnetic field than the other three spacecraft, indicating that C2 did not penetrate as deep into the exhaust as the other spacecraft.

From the observations we can identify that although the current sheet, as defined by the magnetic field reversal (observed at Cluster, ACE, and Wind), is roughly planar on large scales, the trailing edge of the reconnection exhaust at Cluster is not. The spacecraft traversed the current sheet (interval 1) at approximately the same time; however, intervals 2 and 3 are observed at distinctly different times by each spacecraft. Analysis of the time delay between observations of the similar structures by each spacecraft in Figure 5 is used to further constrain the geometry of the current sheet and exhaust in the vicinity of the Cluster spacecraft. The solar wind velocity was used to convert measurements in time into measurements through space, allowing us to identify the spacecraft motion relative to the exhaust. The spacecraft move in a straight line relative to the current sheet at the solar wind velocity (402 km s^{-1}), and the exhaust must have a local geometry which allows the spacecraft to cross its trailing edge at multiple points (the end of interval 1 and the beginning/end of intervals 2 and 3). At the time of observations the four spacecraft were arranged in a straight line such that their motion relative to the solar wind formed a plane. The spatial extents of intervals 1–3, as observed by each spacecraft, are shown in Figure 6. This reconstruction assumes that

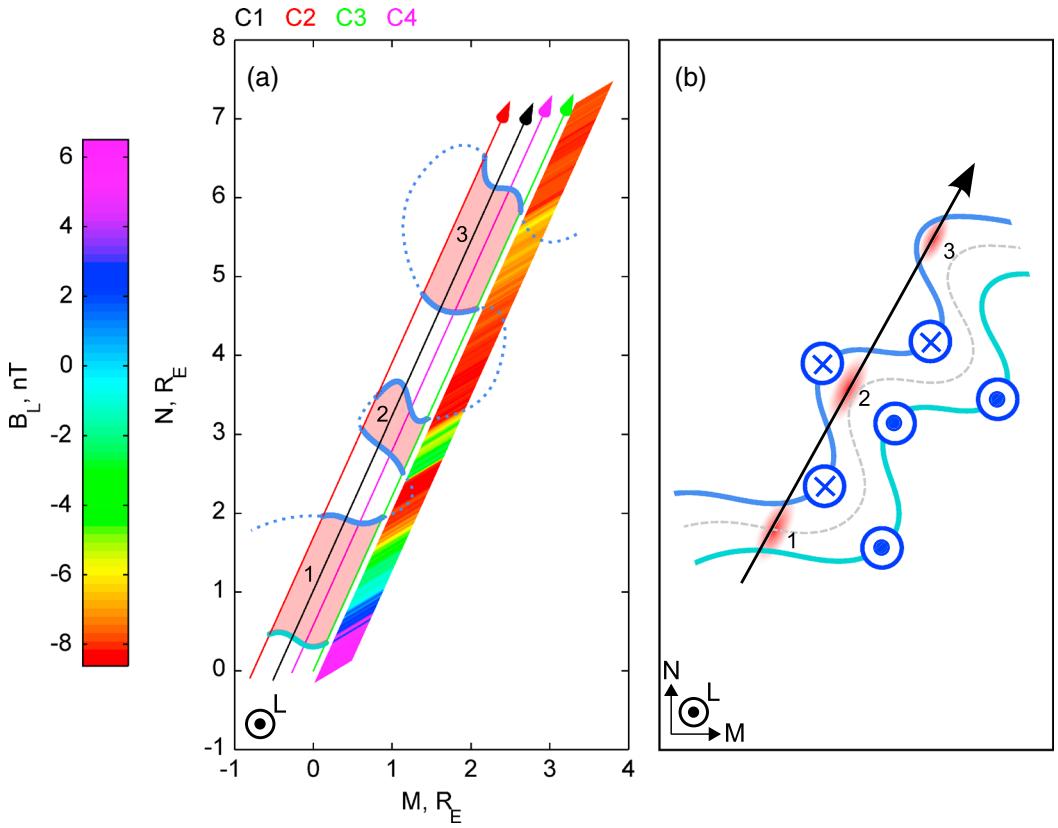

Figure 6. (a) Spatial map of observations of the reconnection exhaust and (b) schematic illustration, both shown in the *MN* plane (the *L* direction is indicated). Note that the spacecraft also move in the +*L* direction, as illustrated in Figure 7. In Figure 6a spacecraft trajectories relative to the exhaust are shown with colored arrows and calculated using a solar wind velocity of 402 km s^{-1}. Positions are relative to C3's position at 09:40:00 UT. C3 measurements of B_L are shown by the color bar. Red shading is used to indicate intervals 1–3. The leading edge of the exhaust is shown in turquoise, the trailing edge in light blue. These edges are calculated by interpolating between the boundaries of intervals 1–3 at each spacecraft. Dotted lines illustrate how the trailing edge may be connected, for comparison with Figure 6b, and are not inferred from the data. The schematic illustration (Figure 6b) shows how intervals 1–3 correspond to distortions in the *MN* plane. The neutral plane at which $B_L = 0$ is in grey and magnetic field directions are shown in dark blue. The black arrow indicates Cluster's motion relative to the exhaust.

the current sheet is frozen to the background solar wind plasma and is not propagating in the solar wind frame. B_L measurements from C3 are also shown, which clearly shows the magnetic field reversal across interval 1 and the change in the magnetic field during intervals 2 and 3.

To constrain the geometry of the reconnection exhaust, we consider distortions from a planar geometry. If distortions were confined to the *LN* plane, the magnetic field at the end of interval 1 and at the beginning/end of intervals 2 and 3 would be expected to have different directions. Figure 3, however, shows that the magnetic field at these exhaust boundaries has the same direction. Similarly, the ion velocity would be expected to have a different direction during each interval; however, it is observed to be mostly in the $-L$ direction. Furthermore, if the exhaust were distorted in such a way, then it is not clear how the flow would interact with the folded exhaust boundaries. The same arguments apply if the distortions were confined to the *LM* plane. The schematic in Figure 6 shows how intervals 1–3 may in fact correspond to distortions in the *MN* plane. In this case the magnetic field has the same orientation at the end of interval 1 and at the beginning/end of intervals 2 and 3, as is observed, and the flow direction is unaffected by the folds as it is perpendicular to the wave vector which describes them. This is consistent with the magnetic field and ion measurements, and therefore suggests that the distortions from a planar geometry are largely confined to the *MN* plane (i.e., perpendicular to both the reconnecting component of the magnetic field and the exhaust outflow). The probability that the spacecraft would intercept a folded current sheet 3 times in this manner

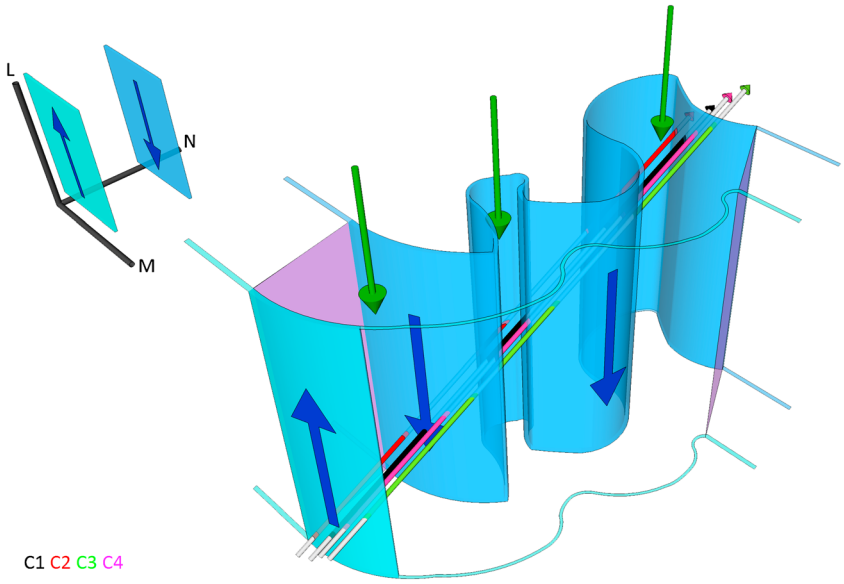

Figure 7. Visualization of the exhaust structure in the vicinity of Cluster, produced using the data from Figure 6. The *LMN* directions are shown. The leading edge of the exhaust is shown in turquoise and the trailing edge in light blue; dark blue arrows on the exhaust edges indicate the local *L* component of the magnetic field. Green arrows indicate the direction of exhaust outflow. Extended arrows indicate spacecraft motion relative to the exhaust, which are colored when the spacecraft are within the exhaust (intervals 1–3 are indicated). Purple edges at either end indicate the exhaust thickness. The orientation of the large-scale current sheet which is detected by ACE, Wind, and Cluster is shown by the small square current sheet edges. A possible leading edge is shown by the turquoise lines to indicate the extent of the exhaust; however, we are unable to constrain its actual shape. Turquoise and light blue lines indicate how this section of the exhaust could connect to the large-scale current sheet.

is extremely low, making this event both remarkable and of particular interest. A 3-D visualization of the local exhaust structure is shown in Figure 7, where we use the positions of the exhaust boundaries as constrained by Figure 6. The visualization shows a possible geometry of the exhaust which is consistent with the observations; however, it is not a unique solution to Figure 6. The geometry of the leading edge of the exhaust (turquoise) can only be constrained near the beginning of interval 1; however, folds in the trailing edge (light blue) are constrained using the end of interval 1 and the beginning/end of intervals 2 and 3. We also note that B_M and B_N are not constant during interval 2 which indicates that there is likely to be some degree of distortion in the *LN* plane, which is not included in the visualization. The likelihood of similar distortions at interval 3 is difficult to determine because changes in the magnetic field are very small. Figure 6 also indicates that distortions in the trailing edge of the current sheet have a length scale of approximately 2.5 R_E (230 d_i).

3. Discussion

Despite the abundance of observational evidence that relatively broad solar wind reconnection exhausts are large scale and roughly planar, simulations and theoretical analysis indicate that exhausts may contain more complicated structure. The observations presented here reveal an extended planar current sheet where observations from Cluster indicate that the trailing edge of the exhaust is folded with length scales of 230 d_i.

The solar wind is inherently turbulent and has a constantly fluctuating magnetic field and velocity. Plasma inflow across the diffusion region and separatricies can therefore be variable in space and time, which could be expected to cause a nonconstant reconnection rate and exhaust width. Variable reconnection rates along the X line may further complicate the exhaust structure in three dimensions. Observations from ACE and Wind indicate that this current sheet was located within the sheath region of an interplanetary shock, where neither ACE nor Wind intercepted the shock driver (e.g., a coronal mass ejection). The plasma surrounding the current sheet may therefore be even more turbulent than average solar wind plasma. Previous studies of reconnection

in stochastically turbulent media have only examined the effects of turbulence near to the X line [*Kowal et al.*, 2009; *Lazarian and Vishniac*, 1999], finding enhanced reconnection rates. Since observations of solar wind reconnection exhausts are likely to be made more than several hundreds of d_i away from the diffusion region [e.g., *Davis et al.*, 2006], the possible effects of turbulence on observed solar wind exhausts are not clear.

Simulations have shown that plasma instabilities can modify a two-dimensional current sheet and cause it to develop more complex three-dimensional structure. A sausage mode results in ballooning of the current sheet thickness (in the *MN* plane), which has been shown to be a primary instability in a 3-D particle-in-cell (PIC) simulation [Büchner and Kuska, 1999]. While similarities can be drawn between this mode and the exhaust geometry which is illustrated in Figure 7, the simulated current sheet only reached the instability threshold once the current sheet thickness was comparable to the ion gyroradius.

The Drift Kink Instability (DKI), driven by relative streaming between ions and electrons, was shown to have predominant modes at $k_M h \approx 1$, where k_M is the wave number, h is the current sheet thickness, and $h = \rho_i$ was assumed (ρ_i is the ion gyroradius) [*Daughton*, 1999]. Using $h = 135\ d_i$ (i.e., the observed current sheet thickness) would imply a wavelength of ~850 d_i. This wavelength is of a similar order of magnitude to the folds which we observe. The instability, however, was shown to have a decreasing growth rate as the sheet thickness and mass ratio m_i/m_e were increased, and it is not expected to be a key instability at $m_i/m_e = 1836$. In this regime the relative streaming of different ion species may become important; however, this instability is expected to grow in current sheets with more significant multi-ion populations, such as the terrestrial magnetotail [*Karimabadi et al.*, 2003].

Simulations of microinstabilities in current sheets typically use thin current sheets (thicknesses of $\sim d_i$) and domains which do not extend far from the diffusion region. We are likely to have observed the exhaust far from the diffusion region, where we have measured the exhaust width to be 135 d_i. The exhaust width is expected to grow with distance from the diffusion region; therefore, the current sheet is likely to be significantly thinner at the diffusion region. It is therefore possible that plasma microinstabilities (e.g., the sausage mode or DKI) may develop at the reconnection site. Furthermore, the observations may have been made a significant time after the onset of reconnection by which point even instabilities with low growth rates may have developed. As with simulations of turbulence, however, instability simulations have not indicated the effects on the exhaust far downstream from the diffusion region. A microinstability whose amplitude and wavelength grows with distance from the diffusion region may be expected to cause a larger macroscale deformation of the current sheet, such as that which we observe. Alternatively, microinstabilities may seed larger-scale instabilities; simulations of the kinetic-scale lower hybrid drift instability (LHDI) have shown that it can induce an ion velocity shear which drives a macroscale Kelvin-Helmholtz instability, causing a large-scale kinking of the current sheet [*Lapenta and Brackbill*, 2002].

Various instabilities can therefore cause a kinking of the current sheet in the *MN* plane on various length scales (e.g., DKI, LHDI, and Kelvin-Helmholtz). Despite evidence that the observed exhaust contains small-scale structure at its trailing edge, the local current sheet normal identified from Cluster during its complete exhaust traversal is closely aligned with the global current sheet normal obtained from the three spacecraft timing analysis. If the exhaust had a local kink structure at Cluster, one might expect that Cluster would cut through the exhaust at a point where the local normal does not match the global normal. This does not, however, rule out the possibility that the current sheet is kinked (indeed in many simulations the dominant instabilities are kink modes), and it appears to be by chance that the two normals are so similar. Moreover, the same plasma instabilities which produce current sheet kinks in idealized simulations may form more unexpected current sheet geometries in real space plasmas, increasing the probability that the local normal at Cluster matches the global normal. Furthermore, the aforementioned instability studies are based on simulations using Harris current sheet configurations, whereas reports of Harris current sheets in the solar wind are rare. The reconnection current sheet in this event is not an ideal Harris current sheet; therefore, while simulations may provide some insight, the particle kinetics are likely to be somewhat different to those that occur in reality. Indeed, while the LHDI developed in a bifurcated current sheet simulation, kink modes with similarities, but notable differences, to the DKI also developed [*Sitnov et al.*, 2004].

Long-wavelength current sheet kinks which have been observed at the magnetotail [e.g., *Sergeev et al.*, 2003; *Volwerk et al.*, 2003] can be compared to the folded current sheet which we observe. These current sheet kinks are associated with reconnection-driven flows and substorm onset. Magnetotail reconnection is bursty,

and multipoint observations indicate that the jets do not extend more than a few R_E perpendicular to the flow [*Nakamura et al*., 2004], while 3-D simulations of magnetotail reconnection show that relatively long wavelength kink instabilities can grow as a consequence of reconnection onset [*Pritchett et al*., 1997]. Our findings may therefore indicate that reconnection in the solar wind and at the magnetotail may be somewhat similar in that they are both capable of forming kinked current sheets. More general three-dimensional simulations have shown that the onset of reconnection is likely to cause a complex current sheet and exhaust structure, before a more planar reconnection exhaust forms [e.g., *Yin et al*., 2008].

Observations at Wind show that it detected the same current sheet as that at Cluster and that it may have detected the reconnection exhaust. If the reconnection exhaust was present at Wind, then it has an increased thickness, stronger guide field (and lower magnetic shear angle), and more variable magnetic field. Cluster and Wind are separated by 320 R_E (29,000 d_i) along the X line (M) direction; therefore, these observations may indicate that the exhaust is variable along its X line, in addition to the small-scale structure which is evident at Cluster.

Without further simulations which focus on the effects of turbulence, instabilities, or other drivers on the exhaust structure, it is difficult to accurately identify the process which caused the observed exhaust to develop its 3-D geometry. Many simulations use low m_i/m_e ratios and have limited domain sizes which do not extend far from the diffusion region and are initialized with no guide field. The observed exhaust exhibited a 122° magnetic shear, and guide fields have been noted to stabilize kink instabilities in some simulations [e.g., *Pritchett and Coroniti*, 2004]. Simulations which can identify indicate how turbulence and instabilities affect the structure of solar wind exhausts further downstream from the diffusion region would be advantageous; however, this presents a significant challenge as the simulations may require large m_i/m_e ratios, moderate guide fields, and large domains. Additionally, although the observed plasma asymmetry on either side of the exhaust is weak (C3 observes $B = 6.6$ nT and $n = 11.9\,\mathrm{cm}^{-3}$ before the exhaust, and $B = 8.5$ nT and $n = 10.7\,\mathrm{cm}^{-3}$ afterward), this kind of asymmetry may warrant further study in the stability analysis of current sheets. Local variations in the ambient plasma's pressure may also exert forces on the exhaust and disturb its structure; however, this has not been studied in simulations.

The observations shown were taken over a total period of 190 s ($t\Omega_i = 128$, where Ω_i is the proton gyrofrequency for $B = 7$ nT). If the trailing edge of the current sheet was not curved and the reencounters were a result of a simple harmonic perturbation to the trailing edge of a current sheet, such that the trailing edge could catch up with the spacecraft as the current sheet was convected past them, the perturbation would require a period of ~60 s ($\omega/\Omega_i = 0.2$) and an amplitude of ~27,000 km (385 d_i). This implies a velocity amplitude of ~2800 km s^{-1}, a velocity far greater than the local sound speed. Such a perturbation would be expected to drive shock waves into the surrounding plasma, which we do not observe. It is important to note, however, that the current sheet may have evolved during a period of $t\Omega_i = 128$. Notably, kinetic kink and tearing instabilities in thin current sheets typically have growth rates $\gamma/\Omega_i < 1$ and frequencies $\omega/\Omega_i < 1$ [*Daughton*, 1999]; therefore, if present they are likely to have changed the current sheet geometry during the observations.

Since solar wind exhausts are rapidly convected past a spacecraft there is a low likelihood that the orientation of a nonplanar exhaust is such that it would be intercepted more than once. It is possible that many of the exhausts which were previously observed could have had small-scale nonplanar features which were not detected. Furthermore, although multispacecraft timing analysis has been used to show that many reconnecting current sheets are planar [e.g., *Phan et al*., 2009], these have used spacecraft which have much larger separations than the length scale of the folds in the current sheet which we detect here. Such methods would be unable to resolve variations from a planar geometry which are of a smaller scale than the spacecraft separations.

4. Conclusions

Using multipoint Cluster observations in conjunction with ACE and Wind, we have identified a solar wind exhaust which is associated with a large-scale current sheet and which exhibits significant small-scale structure. The folds which we detect are likely to be confined to the plane orthogonal to both the reconnecting component of the magnetic field and the exhaust outflow. Numerous current sheet simulations have revealed a variety of kinetic instabilities, some of which can grow to cause large wavelength folds of the

current sheet. Observational data do not allow us to identify instabilities in the observed exhaust; however, 3-D simulations with large domain sizes, moderate guide fields, thick current sheets, and large m_i/m_e ratios may provide further insight.

The observations presented here have important implications for our understanding of solar wind reconnection exhausts and their structure. While reconnection exhausts can often be large scale, planar, and quasi-steady, our observations suggest that they may also contain additional smaller-scale structure and complexity. This has been revealed by a rare and fortuitous encounter where the spacecraft trajectory relative to the exhaust allowed Cluster to intercept the exhaust multiple times, and where timing analysis between the four spacecraft was used to constrain the complex exhaust geometry. Since this kind of encounter is unlikely, it is possible that previously detected large-scale and planar exhausts had small-scale structure at their exhaust boundaries which was left undetected. This possibility invokes the question of how frequently such structuring of reconnection exhausts occurs in the solar wind. This may best be addressed through further simulations or multispacecraft observations using closely spaced spacecraft, such as Cluster and the upcoming Magnetospheric Multiscale mission, which may be able to detect local differences in the current sheet geometry at each spacecraft. Statistical studies of such observations may allow the features of nonplanar solar wind exhausts to be studied further and provide further insight into what conditions lead to their formation.

Acknowledgments

The authors thank Cluster Science Archive (www.cosmos.esa.int/web/csa) and CDAWeb (cdaweb.gsfc.nasa.gov) for providing data which were used in this paper. We thank T. Phan for useful discussions and B. Lavraud for useful comments regarding the use of CIS data. We also thank the reviewers for helpful comments and suggestions. This work was supported by UK STFC through the award of a studentship (R.M.) grant ST/K001051/1 (H.H.) and grant ST/G00725X/1 (J.P.E.). H.H. also thanks the Alfred Kordelin foundation for financial support.

Larry Kepko thanks the reviewers for their assistance in evaluating this paper.

References

Balogh, A., C. Carr, M. Acuna, M. Dunlop, T. Beek, P. Brown, K.-H. Fornacon, E. Georgescu, K.-H. Glassmeier, and J. Harris (2001), The Cluster magnetic field investigation: Overview of in-flight performance and initial results, *Ann. Geophys.*, *19*(10/12), 1207–1217.

Büchner, J., and J. P. Kuska (1999), Sausage mode instability of thin current sheets as a cause of magnetospheric substorms, *Ann. Geophys.*, *17*(5), 604–612.

Daughton, W. (1999), The unstable eigenmodes of a neutral sheet, *Phys. Plasmas*, *6*(4), 1329–1343.

Daughton, W., V. Roytershteyn, H. Karimabadi, L. Yin, B. J. Albright, B. Bergen, and K. J. Bowers (2011), Role of electron physics in the development of turbulent magnetic reconnection in collisionless plasmas, *Nat. Phys.*, *7*(7), 539–542, doi:10.1038/nphys1965.

Davis, M. S., T. D. Phan, J. T. Gosling, and R. M. Skoug (2006), Detection of oppositely directed reconnection jets in a solar wind current sheet, *Geophys. Res. Lett.*, *33*, L19102, doi:10.1029/2006GL026735.

Décréau, P. M. E., et al. (1999), Early results from the Whisper instrument on Cluster: An overview, *Ann. Geophys.*, *19*(10/12), 1241–1258.

Dunlop, M. W., and T. I. Woodward (1998), Multi-spacecraft discontinuity analysis: Orientation and motion, in *Analysis Methods for Multi-Spacecraft Data*, edited by G. Paschmann and P. W. Daly, ESA Publication Division, Netherlands.

Escoubet, C. P., M. Fehringer, and M. Goldstein (2001), Introduction: The cluster mission, *Ann. Geophys.*, *19*(10/12), 1197–1200.

Fujimoto, K. (2009), Fast magnetic reconnection in a kinked current sheet, *Phys. Plasmas*, *16*, 042103, doi:10.1063/1.3106685.

Gosling, J. T. (2007), Observations of magnetic reconnection in the turbulent high-speed solar wind, *Astrophys. J. Lett.*, *671*, L73, doi:10.1086/524842.

Gosling, J. T. (2012), Magnetic reconnection in the solar wind, *Space Sci. Rev.*, *172*(1–4), 187–200, doi:10.1007/s11214-011-9747-2.

Gosling, J. T., and T. D. Phan (2013), Magnetic reconnection in the solar wind at current sheets associated with extremely small field shear angles, *Astrophys. J. Lett.*, *763*(2), L39, doi:10.1088/2041-8205/763/2/L39.

Gosling, J. T., R. M. Skoug, D. J. McComas, and C. W. Smith (2005), Direct evidence for magnetic reconnection in the solar wind near 1 AU, *J. Geophys. Res.*, *110*, A01107, doi:10.1029/2004JA010809.

Gosling, J. T., S. Eriksson, R. M. Skoug, D. J. McComas, and R. J. Forsyth (2006), Petschek-type reconnection exhausts in the solar wind well beyond 1 AU: Ulysses, *Astrophys. J.*, *644*, 613, doi:10.1086/503544.

Gosling, J. T., T. D. Phan, R. P. Lin, and A. Szabo (2007a), Prevalence of magnetic reconnection at small field shear angles in the solar wind, *Geophys. Res. Lett.*, *34*, L15110, doi:10.1029/2007GL030706.

Gosling, J. T., S. Eriksson, T. Phan, D. Larson, R. Skoug, and D. McComas (2007b), Direct evidence for prolonged magnetic reconnection at a continuous X-line within the heliospheric current sheet, *Geophys. Res. Lett.*, *34*, L06102, doi:10.1029/2006GL029033.

Gosling, J. T., S. Eriksson, L. M. Blush, T. D. Phan, J. G. Luhmann, D. J. McComas, R. M. Skoug, M. H. Acuna, C. T. Russell, and K. D. Simunac (2007c), Five spacecraft observations of oppositely directed exhaust jets from a magnetic reconnection X-line extending $> 4.26 \times 106$ km in the solar wind at 1 AU, *Geophys. Res. Lett.*, *34*, L20108, doi:10.1029/2007GL031492.

Horbury, T. S., D. Burgess, M. Fränz, and C. J. Owen (2001), Three spacecraft observations of solar wind discontinuities, *Geophys. Res. Lett.*, *28*(4), 677–680, doi:10.1029/2000GL000121.

Hudson, P. D. (1970), Discontinuities in an anisotropic plasma and their identification in the solar wind, *Planet. Space Sci.*, *18*(11), 1611–1622.

Karimabadi, H., W. Daughton, P. L. Pritchett, and D. Krauss-Varban (2003), Ion-ion kink instability in the magnetotail: 1. Linear theory, *J. Geophys. Res.*, *108*(A11), 1400, doi:10.1029/2003JA010026.

Kowal, G., A. Lazarian, E. T. Vishniac, and K. Otmianowska-Mazur (2009), Numerical tests of fast reconnection in weakly stochastic magnetic fields, *Astrophys. J.*, *700*, 63, doi:10.1088/0004-637X/700/1/63.

Lapenta, G., and J. U. Brackbill (2002), Nonlinear evolution of the lower hybrid drift instability: Current sheet thinning and kinking, *Phys. Plasmas*, *9*(5), 1544–1554.

Lazarian, A., and E. T. Vishniac (1999), Reconnection in a weakly stochastic field, *Astrophys. J.*, *517*(2), 700.

Le, A., J. Egedal, J. Ng, H. Karimabadi, J. Scudder, V. Roytershteyn, W. Daughton, and Y.-H. Liu (2014), Current sheets and pressure anisotropy in the reconnection exhaust, *Phys. Plasmas*, *21*, 012103, doi:10.1063/1.4861871.

Lin, R. P., et al. (1995), A three-dimensional plasma and energetic particle investigation for the wind spacecraft, *Space Sci. Rev.*, *71*(1–4), 125–153.

Liu, Y.-H., J. F. Drake, and M. Swisdak (2012), The structure of the magnetic reconnection exhaust boundary, *Phys. Plasmas*, *19*, 022110, doi:10.1063/1.4840015.

McComas, D. J., S. J. Bame, P. Barker, W. C. Feldman, J. L. Phillips, P. Riley, and J. W. Griffee (1998), Solar Wind Electron Proton Alpha Monitor (SWEPAM) for the Advanced Composition Explorer, *Space Sci. Rev.*, *86*(1–4), 563–612.

Merka, J., A. Szabo, J. A. Slavin, and M. Peredo (2005), Three-dimensional position and shape of the bow shock and their variation with upstream Mach numbers and interplanetary magnetic field orientation, *J. Geophys. Res.*, *110*, A04202, doi:10.1029/2004JA010944.

Nakamura, R., et al. (2004), Spatial scale of high-speed flows in the plasma sheet observed by Cluster, *Geophys. Res. Lett.*, *31*, L09804, doi:10.1029/2004GL019558.

Ogilvie, K. W., et al. (1995), SWE, a comprehensive plasma instrument for the WIND spacecraft, *Space Sci. Rev.*, *71*(1–4), 55–77.

Osman, K. T., W. H. Matthaeus, J. T. Gosling, A. Greco, S. Servidio, B. Hnat, S. C. Chapman, and T. D. Phan (2014), Magnetic reconnection and intermittent turbulence in the solar wind, *Phys. Rev. Lett.*, *112*, doi:10.1103/PhysRevLett.112.215002.

Paschmann, G., I. Papamastorakis, W. Baumjohann, N. Sckopke, C. W. Carlson, B. U. Ö. Sonnerup, and H. Lühr (1986), The magnetopause for large magnetic shear: AMPTE/IRM observations, *J. Geophys. Res.*, *91*(A10), 11,099–11,115.

Phan, T. D., et al. (2006), A magnetic reconnection X-line extending more than 390 Earth radii in the solar wind, *Nature*, *439*(7073), 175–178, doi:10.1038/nature04393.

Phan, T. D., J. T. Gosling, and M. S. Davis (2009), Prevalence of extended reconnection X-lines in the solar wind at 1 AU, *Geophys. Res. Lett.*, *36*, L09108, doi:10.1029/2009GL037713.

Pritchett, P. L., and F. V. Coroniti (2004), Three-dimensional collisionless magnetic reconnection in the presence of a guide field, *J. Geophys. Res.*, *109*, A01220, doi:10.1029/2003JA009999.

Pritchett, P. L., F. V. Coroniti, and R. Pellat (1997), Convection-driven reconnection and the stability of the near-Earth plasma sheet, *Geophys. Res. Lett.*, *24*(8), 873–876, doi:10.1029/97GL00672.

Reme, H., C. Aoustin, J. Bosqued, I. Dandouras, B. Lavraud, J. Sauvaud, A. Barthe, J. Bouyssou, T. Camus, and O. Coeur-Joly (2001), First multispacecraft ion measurements in and near the Earth's magnetosphere with the identical Cluster ion spectrometry (CIS) experiment, *Ann. Geophys.*, *19*(10/12), 1303–1354.

Sergeev, V., et al. (2003), Current sheet flapping motion and structure observed by Cluster, *Geophys. Res. Lett.*, *30*(6), 1327, doi:10.1029/2002GL016500.

Sitnov, M., M. Swisdak, J. Drake, P. Guzdar, and B. Rogers (2004), A model of the bifurcated current sheet: 2. Flapping motions, *Geophys. Res. Lett.*, *31*, L09805, doi:10.1029/2004GL019473.

Sonnerup, B., and L. J. Cahill (1967), Magnetopause structure and attitude from Explorer 12 observations, *J. Geophys. Res.*, *72*(1), 171–183, doi:10.1029/JZ072i001p00171.

Vasyliunas, V. M. (1975), Theoretical models of magnetic field line merging, *Rev. Geophys.*, *13*(1), 303–336, doi:10.1029/RG013i001p00303.

Volwerk, M., K. H. Glassmeier, A. Runov, W. Baumjohann, R. Nakamura, T. L. Zhang, B. Klecker, A. Balogh, and H. Rème (2003), Kink mode oscillation of the current sheet, *Geophys. Res. Lett.*, *30*(6), 1320, doi:10.1029/2002GL016467.

Yin, L., W. Daughton, H. Karimabadi, B. J. Albright, K. J. Bowers, and J. Margulies (2008), Three-dimensional dynamics of collisionless magnetic reconnection in large-scale pair plasmas, *Phys. Rev. Lett.*, *101*(12), 125001, doi:10.1103/physrevlett.101.125001.

Zweibel, E. G., and M. Yamada (2009), Magnetic reconnection in astrophysical and laboratory plasmas, *Annu. Rev. Astron. Astrophys.*, *47*, 291–332, doi:10.1146/annurev-astro-082708-101726.